Industrial Crops & Products 223 (2025) 120126

Contents lists available at ScienceDirect

Industrial Crops & Products

journal homepage: www.elsevier.com/locate/indcrop

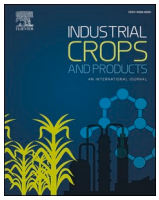

Insights into the interactions between cellulose and hemicellulose during pyrolysis for optimizing the properties of biochar as a potential energy vector

Xiaoran Li [a], Kehui Cen [a], Jinjin Li [a], Dongxia Jia [a], Jiangyong Gao [b,*], Liqiang Zhang [c], Dengyu Chen [a,*]

[a] Co-Innovation Center of Efficient Processing and Utilization of Forest Resources, College of Materials Science and Engineering, Nanjing Forestry University, Nanjing 210037, China
[b] Higher Education Research Institute, Nanjing Forestry University, Nanjing 210037, China
[c] College of New Energy, China University of Petroleum (East China), Qingdao, Shandong 266580, China

ARTICLE INFO

Keywords:
Biochar
Cellulose
Hemicellulose
Pyrolysis
Response surface methodology

ABSTRACT

Cellulose and hemicellulose, the main components of biomass, undergo noticeable interactions during biomass pyrolysis. In this study, biochar was produced by the co-pyrolysis of cellulose and hemicellulose. Three co-pyrolysis parameters, namely, pyrolysis temperature (400–800 °C), residence time (5–30 min), and percentage of cellulose (0–100 %), were investigated to optimize the properties of biochar, including the application of response surface methodology in the experimental study. The analysis revealed that co-pyrolysis interactions could improve the biochar yield by up to 41.37 % (567.74 °C, 19.52 min, 50 % cellulose percentage). The co-pyrolysis interactions specifically enhanced the fixed carbon content, elemental carbon content, and higher heating value of the biochar, with the most significant enhancements being 0.87 %, 3.60 %, and 3.85 %, respectively, while simultaneously decreasing the volatile content, [H]/[C] ratio, and [O]/[C] ratio of the biochar, with the most significant reductions of −9.30 %, −10.81 %, and −26.71 %. Based on the observed decrease in the intensity ratio of the D-band and G-band of biochar in the Raman spectra, greater co-pyrolysis interactions increased the graphitization degree of the biochar. The analysis of X-ray photoelectron spectroscopy (XPS) investigations revealed that the interactions enhanced the contents of the C-C, C-O/C-O-C, aromatic, and OH functionalities while reducing the number of COO-, COOH, and C═O functional groups. The results of this work indicate that the co-pyrolysis interaction between cellulose and hemicellulose contributes to optimizing the properties of biochar as a potential energy vector.

1. Introduction

Biomass is an important resource in the global energy system due to its sustainability and ability to reduce carbon emissions (Wu et al., 2023). As biomass consists of complex polymeric structures, its pyrolysis process is complex and difficult to be directly used as the research subject to comprehensively explore the principles of biomass pyrolysis (Cai et al., 2024; Wang et al., 2023a). Biomass consists of three main components: cellulose, hemicellulose, and lignin (Ma et al., 2024). Compared to lignin, cellulose and hemicellulose have higher reactivity, lower thermal stability, and can be more quickly decomposed into volatile products (Chen et al., 2017; Zhu et al., 2024). During the pyrolysis process, cellulose and hemicellulose have partially overlapping pyrolysis temperature ranges and produce some identical pyrolysis products, leading to their interactions during the pyrolysis process (Hu et al., 2024). Therefore, a deeper understanding of the interactions between cellulose and hemicellulose is essential for a better understanding of the pyrolysis principles.

In recent years, pyrolysis of cellulose and hemicellulose has been extensively studied by many researchers. At low pyrolysis temperatures, cellulose primarily undergoes depolymerization and dehydration reactions, resulting in products dominated by levoglucosan and other dehydrated sugars (Zhao et al., 2024). With increasing temperature, the chemical bonds of levoglucosan and other dehydrated sugars break

* Corresponding authors.
E-mail addresses: gjy@njfu.edu.cn (J. Gao), chendy@njfu.edu.cn (D. Chen).

https://doi.org/10.1016/j.indcrop.2024.120126
Received 4 October 2024; Received in revised form 12 November 2024; Accepted 19 November 2024
Available online 26 November 2024

down, generating numerous small molecular products (Liu et al., 2023; Wang et al., 2024). While the pyrolysis processes of hemicellulose and cellulose are similar, hemicellulose does not produce intermediate products similar to levoglucosan at low temperatures and is more prone to dehydration reactions in the subsequent pyrolysis stages.

Couhert et al. studied the product distribution during co-pyrolysis of cellulose and hemicellulose by pyrolysis gas chromatography-coupled mass spectrometry (Py-GC/MS). The authors observed that the co-pyrolysis interactions were the strongest at about 500 °C, weakened slightly at about 600 °C, and strengthened again at about 700 °C (Couhert et al., 2009). Hosoya et al. also found that the co-pyrolysis of cellulose and hemicellulose resulted in a generation of cellulose decomposition products such as glycolaldehyde, levoglucosan, and 1, 4:3,6-dianhydroglucopyranose that was lower than predicted (Hosoya et al., 2007). In contrast, the yields of hemicellulose-related products were higher than expected. To date, most of the published research on the co-pyrolysis interactions between cellulose and hemicellulose has primarily focused on the analysis of liquid products, while studies on solid products and their physicochemical properties have been relatively scarce.

The solid product of the co-pyrolysis of cellulose and hemicellulose is biochar. The physicochemical properties of biochar determine its thermal stability, combustion performance, and suitability as an energy source (Mao et al., 2023; Wang et al., 2023b). Furthermore, the properties and yields of biochar are significantly influenced by factors such as co-pyrolysis temperature, time, and the ratio of feedstocks (Yang et al., 2023). During the pyrolysis process, elevated temperatures typically cause biochar yields to decline, yet simultaneously enhance its thermal stability (Guo et al., 2024). Shorter pyrolysis times can retain more volatile components, while longer times promote the completion of pyrolysis reactions, thereby producing more stable biochar. Additionally, the ratio of cellulose to hemicellulose can influence the elemental composition and properties of the resulting biochar. Conventional analytical methods cannot simultaneously analyze the effects of the above three pyrolysis parameters on biochar. Response surface methodology (RSM) combines mathematical and statistical tools to optimize experimental conditions and study the effect of interactions on the outcomes of the experiment (Ba et al., 2023; Zalazar-Garcia et al., 2022). This approach has been applied to study the interactions between eucalyptus and sodium polyacrylate (Singh et al., 2020), as well as between purun tikus and plastic waste (Amrullah et al., 2024). Nevertheless, there are few reports on the effect of co-pyrolysis interactions on yields and the physicochemical and structural properties of biochar from cellulose and hemicellulose.

In this study, cellulose and hemicellulose were used as feedstock materials to produce biochar through co-pyrolysis and to conduct process optimization based on RSM. This study aims to evaluate the impact of co-pyrolysis interactions between cellulose and hemicellulose on key physicochemical properties of the resultant biochar, specifically targeting fixed carbon content, elemental carbon content, and higher heating value (HHV). The co-pyrolysis interaction not only improves the yield of biochar but also optimizes its carbon content, providing a new and theoretical basis for improving the performance of biochar in energy applications.

2. Materials and methods

2.1. Materials

Microcrystalline cellulose from Sigma-Aldrich (product number 435236, white powder) and xylan (CAS no. 9014-63-5, white powder from corn cob) from Aladdin Reagent Co., Ltd., were used in this study. The basic properties of the specimens are presented in Table S1.

2.2. Experiments and characterization

The experimental setup (VTL1200–1200, Bojunton, China) consisting of a vertical furnace is shown in Fig. S1. The experiment was performed under nitrogen as the protective gas with a flow rate of 300 mL per minute. A crucible containing 4 g of the sample was placed at the top of a quartz tube and exposed to a nitrogen atmosphere for 15 min. Once the furnace temperature reached the preset value, the crucible was slowly lowered into the pyrolysis zone in the middle of the quartz tube. After completion of the experiment, the crucible was removed, and the sample was allowed to cool. The biochar yield was determined by calculating the ratio of the mass of the residual material in the crucible to the initial feedstock mass.

This study uses the central composite design (CCD) method of RSM to design the experiments. Three factors, namely, pyrolysis temperature (A, 400–800 °C), residence time (B, 5–30 min), and cellulose percentage (C, 0–100%) were examined. Table S2 provides the correspondence between the coded and actual values of the experimental variables. The experimental parameters and obtained biochar yields are listed in Table 1. The HHV, proximate analysis, and ultimate analysis results of the biochar obtained from the co-pyrolysis experiments are presented in Table 2, while the [H]/[C] and [O]/[C] ratios are provided in Table S3, and the XPS results are shown in Table S4. The analysis of variance is provided in Table S5. Details of biochar characterization (ultimate analysis, proximate analysis, HHV, Raman, and XPS) are provided in the Supplementary Material.

The impact of co-pyrolysis interactions on biochar yield and its characteristics is calculated using Eq. (1). The calculated value is obtained using Eq. (2).

$$SE(\%) = \frac{X_{\exp} - X_{cal}}{X_{cal}} \times 100\% \quad (1)$$

$$X_{cal} = \alpha\omega_c + \beta\omega_L \quad (2)$$

where SE represents the relative deviation between the experimental and calculated values of biochar yield and its characterization. A positive relative deviation suggests that the co-pyrolysis interactions have a beneficial effect on the biochar yields and its characteristics, whereas a negative deviation suggests an inhibitory effect. $X_{\exp}$ and X_{cal} represent experimental and calculated values of biochar yield and each characteristic under different influencing factors. The mass proportions of cellulose and hemicellulose in the raw material are represented by α and β, respectively. ω_c and ω_L are performance data obtained by individual

Table 1
Experimental design matrix and obtained biochar yields.

Run	A: Pyrolysis temperature (°C)	B: Residence time (min)	C: Percentage of cellulose (%)	Biochar yield (wt%)
1	720	25	20	8.15
2	600	17.5	50	14.64
3	720	10	80	8.31
4	720	25	80	8.25
5	600	17.5	50	14.40
6	600	17.5	0	8.75
7	480	10	20	15.46
8	480	25	80	18.07
9	600	17.5	50	15.01
10	480	25	20	14.28
11	800	17.5	50	10.89
12	600	17.5	50	15.18
13	600	17.5	50	14.80
14	600	17.5	50	14.50
15	480	10	80	19.43
16	400	17.5	50	25.14
17	600	5	50	14.98
18	600	30	50	14.84
19	600	17.5	100	12.01
20	720	10	20	10.11

Table 2
The HHV, proximate analysis, ultimate analysis, and Raman spectroscopy results of biochar by co-pyrolysis experiment.

Run	HHV (MJ/kg)	[C] (wt%, db)	[H] (wt%, db)	[O]* (wt%, db)	Volatiles (wt%, db)	Fixed carbon (wt%, db)	I_D/I_G
1	31.53	85.89	1.35	12.76	4.43	95.57	4.06
2	32.36	86.62	2.30	11.08	8.68	91.32	8.13
3	33.74	90.87	1.81	7.32	5.82	94.18	4.39
4	33.05	89.27	1.75	8.98	5.79	94.21	4.21
5	32.48	86.88	2.36	10.77	8.89	91.11	7.41
6	30.46	81.95	2.18	15.87	8.58	91.42	4.86
7	29.97	78.81	3.41	17.78	20.29	79.71	14.39
8	30.07	79.48	3.16	17.36	20.02	79.98	14.48
9	32.42	81.62	2.42	15.97	8.78	91.22	7.30
10	29.48	78.85	2.56	18.59	17.78	82.22	13.90
11	33.45	91.21	1.11	7.68	4.09	95.91	3.95
12	32.71	87.48	2.34	10.18	9.19	90.81	8.63
13	32.80	87.59	2.41	10.00	9.02	90.98	7.69
14	33.28	88.87	2.36	8.77	9.11	90.89	7.82
15	30.35	79.88	3.34	16.78	23.35	76.65	18.02
16	29.28	76.3	3.91	19.79	30.88	69.12	18.84
17	29.41	76.65	3.88	19.47	10.09	89.91	20.84
18	32.10	89.14	2.39	8.47	8.14	91.86	4.83
19	32.86	87.18	2.59	10.07	10.80	89.20	14.18
20	31.21	83.91	2.15	13.94	5.14	94.86	4.16

* Oxygen was estimated by the difference.

pyrolysis experiments of cellulose and hemicellulose, respectively. The biochar yield, HHV, proximate analysis, ultimate analysis, Raman spectroscopy, and XPS results of biochar obtained from the individual pyrolysis of cellulose and hemicellulose are represented as Run X (1−16) and are presented in Tables S6 and S7.

3. Results and discussion

3.1. Effect of co-pyrolysis interactions on biochar yield

Fig. 1(a)–(c) compares three different sets of conditions, each resulting in a peak SE value, which indicates that these specific conditions maximize the beneficial effect of co-pyrolysis on biochar yield. Colors ranging from blue (lower relative deviations) to red (higher relative deviations) represent different levels of relative deviations. The color bar on the right indicates the numerical values of the relative deviations (SE) of the biochar yields from the calculated values. The highest SE value reflects the strongest positive impact of co-pyrolysis on biochar yields. The co-pyrolysis interactions had a noticeable positive impact on biochar yield. As shown in Fig. 1(a), SE reached its maximum value of 41.37 % at a fixed cellulose percentage of 50 %, a temperature of 567.74 °C, and a time of 19.52 min. As depicted in Fig. 1(b), with a fixed time of 17.5 min, a cellulose percentage of 48.39 %, and a temperature of 580.65 °C, the SE value reached its highest point at 40.93 %. Similarly, as illustrated in Fig. 1(c), with a fixed temperature of 600 °C, a time of 18.71 min, and a cellulose percentage of 45.03 %, SE had its highest value at 40.73 %. These observations were similar to those reported by Torres-Sciancalepore et al. (Torres-Sciancalepore et al., 2024).

These results can be attributed to the fact that hemicellulose is thermally less stable than cellulose, leading to the formation of products from feedstock in a molten state during pyrolysis at low temperatures (Hosoya et al., 2007). These products cover the cellulose surface to form liquid-solid interfaces, which inhibit the pyrolysis of cellulose into small-molecule liquid and gaseous products and lead to an increase in solid residues (Kawamoto, 2015; Xu et al., 2020a). As pyrolysis progresses, the formation of liquid cellulose subsequently triggers the liquid-liquid interactions between molten hemicellulose and cellulose. This dual interaction mechanism promotes the formation of biochar (Zalazar-Garcia et al., 2024; Zhang et al., 2024).

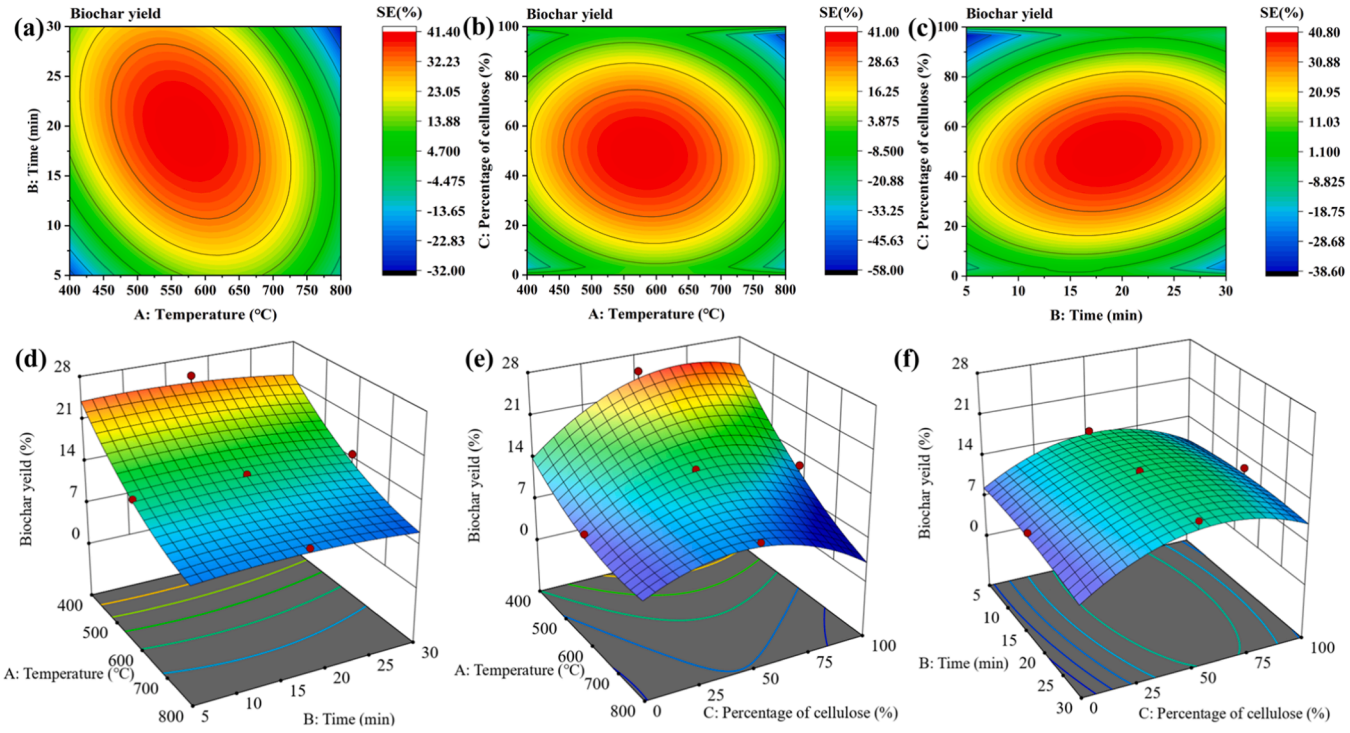

Fig. 1. Effect of co-pyrolysis interactions on biochar yield at (a) temperature vs. time (50 % cellulose), (b) temperature vs. cellulose percentage (17.5 min), and (c) time vs. cellulose percentage (600 °C); biochar yield 3D surface simulation at (d) temperature vs. time (50 % cellulose), (e) temperature vs. cellulose percentage (17.5 min), and (f) time vs. cellulose percentage (600 °C).

3.2. Effects of three co-pyrolysis factors on biochar yield

The impact of the three factors on the biochar yields from the co-pyrolysis of cellulose and hemicellulose is shown in Fig. S2. The steepness of the curves reflects the impact of each factor on biochar yield. The analysis showed that factor A had the greatest effect, followed by factor C, while factor B had the least impact on biochar yield. According to Eq. (3), A and B had negative effects on biochar yield while C had a beneficial effect.

$$\text{Biochar yield} = +14.82 - 4.08\,A - 0.3263B + 0.8644\,C + 0.1043AB - 1.12AC + 0.2517BC + 0.8090\,A^2 - 0.2887B^2 - 1.89\,C^2 \quad (3)$$

Fig. 1(d)–(f) depicts the effect of the three factors on biochar yield. As illustrated in Fig. 1(d), when the cellulose percentage was 50 %, increasing the temperature from 400 °C to 800 °C resulted in a decrease in biochar yield with the yield dropping from 24.00 wt% to 9.68 wt% at a pyrolysis time of 5 min and from 22.32 wt% to 9.17 wt% at a time of 30 min. The reduction in biochar production at higher temperatures is due to the intensified cracking reactions of cellulose and hemicellulose, producing more gaseous and liquid products (Xing et al., 2023; Yang et al., 2007). Fig. 1(e) shows the impact of changes in temperature and cellulose percentage on biochar yield at a fixed pyrolysis time of 17.5 min. When the pyrolysis temperature was 400 °C, the biochar yield improved with increasing cellulose percentage, but when the pyrolysis temperature was 800 °C, the change in cellulose percentage had a negligible effect on biochar yield. As a reason for the smaller impact at a higher pyrolysis temperature, both cellulose and hemicellulose undergo nearly complete pyrolysis under these conditions, reducing the sensitivity of the biochar yield to changes in cellulose content (Quan et al., 2016). Fig. 1(f) indicated that changes in cellulose percentage and residence time exhibited a minimal impact on biochar yield at a fixed temperature of 600 °C. The maximum biochar yield at 13.93 min and a cellulose percentage of 55.85 % was 14.99 wt%. At 18.23 min and a cellulose percentage of 0.59 %, the maximum biochar yield was 8.09 wt %.

3.3. Proximate analysis

Fig. 2(a)–(c) shows the impact of co-pyrolysis interactions on the volatile products of the pyrolysis. The SE values were negative under the specified conditions, suggesting an inhibitory effect of the co-pyrolysis interactions on the formation of volatile content. Specifically, the conditions corresponding to these negative SE values were (1) a fixed cellulose percentage of 50 %, a temperature range from 434.78 to 699.24 °C, and pyrolysis times from 5 to 30 min (Fig. 2(a)); (2) a fixed residence time of 17.5 min, a temperature range from 438.48 to 713.04 °C, and cellulose percentages from 0.74 % to 90.24 % (Fig. 2(b)); (3) a fixed pyrolysis temperature of 600 °C, a residence time from 5 to 30 min, and a cellulose percentage from 1.69 % to 77.39 % (Fig. 2(c)). Fig. 2(c) shows that, with a fixed pyrolysis temperature of 600 °C, a residence time of 21.94 min, and a cellulose percentage of 38.71 %, the SE value reached its minimum at –9.30 %, indicating that the inhibitory effect on volatile content production is the strongest under these conditions. This can be explained by the fact that during pyrolysis, hemicellulose melts before cellulose, wrapping cellulose and inhibiting the formation of volatiles from cellulose (Hosoya et al., 2007).

Fig. 2(d)–(f) illustrates the effect of co-pyrolysis interactions on the fixed carbon content of the biochar. The co-pyrolysis interactions had a slight positive impact on the fixed carbon content of the biochar. The three conditions corresponding to the strongest positive effect can be summarized as (1) a fixed cellulose percentage of 50 %, a temperature of 606.54 °C, and a time of 21.13 min, resulting in an SE peak value of 0.87 % (Fig. 2(d)); (2) a fixed residence time of 17.5 min, a temperature of 606.54 °C, and a cellulose percentage of 45.16 %, where the SE value reached its highest point at 0.86 % (Fig. 2(e)); (3) a fixed pyrolysis temperature of 600 °C, a residence time of 21.13 min, and a cellulose percentage of 45.16 %, leading to a maximum SE value of 0.87 % (Fig. 2 (f)). As previously discussed, these interactions suppress the formation of volatiles in the biochar, thereby indirectly promoting the accumulation of fixed carbon in the biochar (Zhou et al., 2018).

Eqs. (4) and (5) represent the models for predicting fixed carbon content and volatile content, respectively. Based on the equations, increases in A and B were found to have a favorable impact on the fixed carbon content, while increasing C significantly decreased the fixed carbon content. These trends of the three factors were opposite for the volatile content since complete pyrolysis occurred as temperature and time increased, resulting in the breakdown of a significant amount of organic matter into smaller molecules. This led to the release of greater

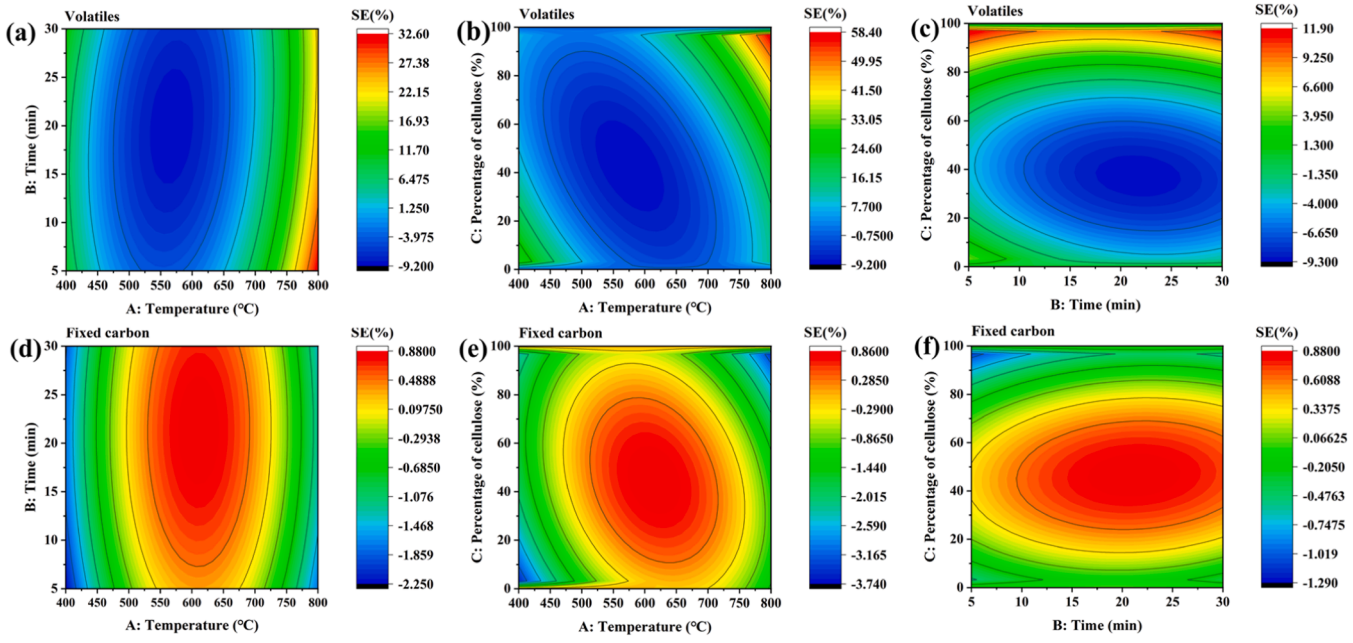

Fig. 2. Effect of co-pyrolysis interactions on volatile contents (a–c), and fixed carbon content (d–f): (a, d) temperature vs. time (cellulose percentage 50 %); (b, e) temperature vs. cellulose percentage (17.5 min); (c, f) time vs. cellulose percentage (600 °C).

quantities of volatile compounds (such as CO, CO_2, H_2O, hydrocarbons, alcohols, etc.) from the feedstock (Cen et al., 2022). Consequently, the decreased volatile content in the biochar indicated that it was converted into gaseous products rather than remaining in the biochar (Zhao et al., 2018).

$$\text{Fixed carbon} = +91.07 + 7.67A + 0.7186B - 0.8071C - 0.6261AB + 0.4002AC + 0.0172BC - 3.12A^2 - 0.1622B^2 - 0.3655C^2 \quad (4)$$

$$\text{Volatile contents} = +8.93\,B - 7.67A - 0.7186B + 0.8071C + 0.6261AB - 0.4002AC - 0.0172BC + 3.12A^2 + 0.1622B^2 + 0.3655C^2 \quad (5)$$

3.4. Ultimate analysis

3.4.1. Carbon content

Fig. 3(a)–(c) illustrates the effect of co-pyrolysis interactions on elemental carbon. It could be concluded that the co-pyrolysis interactions moderately improved the carbon content of the biochar. The three conditions under which the interactions positively affected the carbon content can be summarized as: (1) temperatures ranging from 400.00 to 786.84 °C and times from 8.07 to 27.07 min at a fixed cellulose percentage of 50 %, resulting in positive SE values (Fig. 3(a)); (2) at a fixed time of 17.5 min, temperatures ranging from 408.29 to 791.60 °C and cellulose percentages from 8.29 % to 98.67 %, where the SE values were positive (Fig. 3(b)); (3) at a fixed pyrolysis temperature of 600 °C, a residence time from 5.73 to 28.36 min and a cellulose percentage from 9.85 % to 99.03 % (Fig. 3(c)). Fig. 3(c) illustrates that, with a fixed temperature of 600 °C, a time of 17.10 min, and a cellulose percentage of 64.52 %, the SE value reached its maximum of 3.60 %, indicating the strongest positive effect on the carbon content. This can be attributed to the co-pyrolysis interactions, which promote cellulose in the biochar better to retain its carbon content under pyrolysis conditions, thereby increasing the proportion of carbon in the final product (He et al., 2024). Eq. (6) represents the models of the carbon content in biochar, revealing that increasing the pyrolysis temperature and residence time exhibits a favorable effect on carbon content while raising the cellulose percentage has an adverse impact on carbon content.

$$\text{Carbon content} = +68.45 + 2.85A + 0.153B - 4.81C - 0.0675AB - 0.0356AC - 0.3327BC - 1.6A^2 - 0.8860B^2 + 1.92C^2 \quad (6)$$

3.4.2. [H]/[C] molar ratio

Fig. 3(d)–(f) illustrates the effect of co-pyrolysis interactions on the [H]/[C] ratio. The [H]/[C] ratios are provided in Table S3. Co-pyrolysis interactions led to a reduction in the [H]/[C] ratio of the biochar. The conditions corresponding to negative SE values were (1) at a fixed cellulose percentage of 50 %, a temperature range of 404.13–671.74 °C and a time range of 13.69–28.90 min (Fig. 3(d)); (2) when the time was fixed at 17.5 min, temperature and cellulose percentage ranges of 404.13–687.39 °C and 1.70 %–98.53 %, respectively (Fig. 3(e)); (3) at a

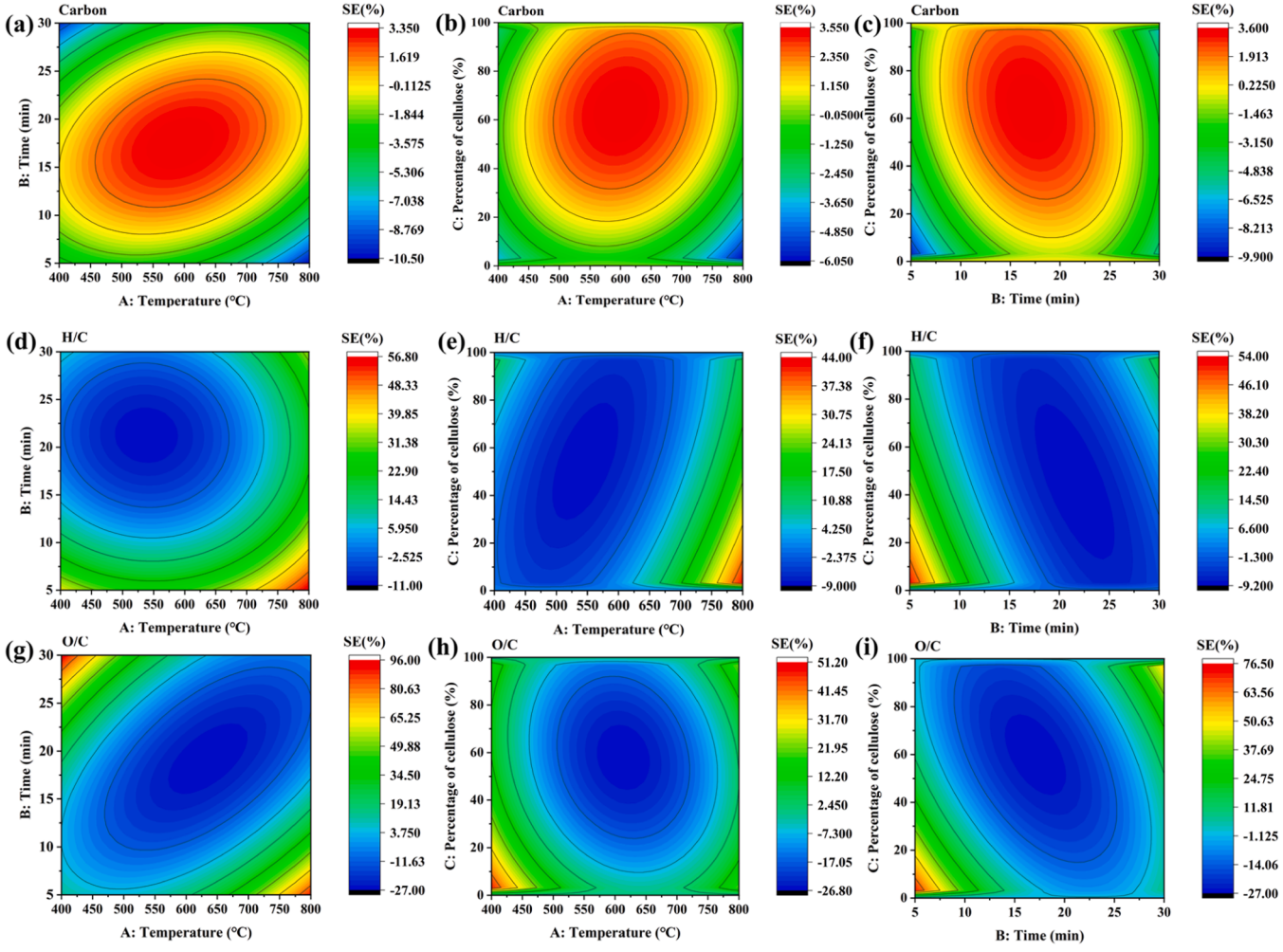

Fig. 3. Effect of co-pyrolysis interactions on carbon content (a–c), [H]/[C] ratio (d–f), and [O]/[C] ratio (g–i): (a, d, g) temperature vs. time (cellulose percentage 50 %); (b, e, h) temperature vs. cellulose percentage (17.5 min); (c, f, i) time vs. cellulose percentage (600 °C).

temperature of 600 °C, a time range of 12.23–30.00 min and a cellulose percentage range of 0.40 %–99.18 % (Fig. 3(f)). According to Fig. 3(d), when the cellulose percentage was 50 %, the SE value was the lowest at –10.81 % at a temperature of 541.93 °C and a time of 21.13 min, indicating the strongest inhibitory effect. Eq. (7) is a model for the [H]/[C] ratio of the biochar. It was found that an increase in time and temperature reduced the [H]/[C] ratio, while a higher cellulose percentage increased the ratio. This suggests that the [H]/[C] ratio can be adjusted by modifying the pyrolysis conditions, thereby altering the aromaticity of the biochar to meet the needs of various applications (Wang et al., 2022).

$$[H]/[C] = +0.3270 - 0.1238A - 0.0551B + 0.0110C + 0.0037AB - 0.0110AC + 0.0282BC + 0.0111A^2 + 0.0394B^2 - 0.0012C^2 \quad (7)$$

3.4.3. [O]/[C] molar ratio

Fig. 3(g)–(i) illustrates the effect of co-pyrolysis interactions on the [O]/[C] ratio. The [O]/[C] ratios are provided in Table S3. Co-pyrolysis interactions led to a reduction in the [O]/[C] ratio of biochar. The conditions corresponding to negative SE values were as follows: (1) at a fixed cellulose percentage of 50 %, a temperature range of 400.00–800.00 °C and time range of 5.56–30.00 min (Fig. 3(g)); (2) at a time of 17.5 min, a temperature range of 459.79–764.35 °C and cellulose percentage range of 9.68 %–98.53 % (Fig. 3(h)); (3) at a temperature of 600 °C, a time range and cellulose percentage range of 5.41–28.63 min and 0.74 %–98.22 %, respectively (Fig. 3(i)). According to Fig. 3(g), the SE value was the lowest at –26.65 % for a cellulose percentage fixed at 50 % when a temperature and time of 632.26 °C and 19.52 min was employed, indicating that at this time the co-pyrolysis interaction had the strongest reduction impact on the [O]/[C] ratio. Eq. (8) is a model for the [O]/[C] ratio of biochar. A rise in temperature, time, and cellulose percentage resulted in a decrease in the [O]/[C] ratio.

$$[O]/[C] = +0.0882 - 0.0378A - 0.0132B - 0.0161C + 0.0000AB - 0.0074AC + 0.0025BC + 0.0134A^2 + 0.0152B^2 + 0.0116C^2 \quad (8)$$

In this study, a Van-Krevelen diagram was used to characterize the [H]/[C] and [O]/[C] ratios of biochar, as shown in Fig. 4. The diagram displays the [H]/[C] and [O]/[C] ratios of biochar pyrolysis samples (Runs 1–20), where the samples located in the dashed box (Runs 3, 4, 5, 9, 11, 12, 13, 14, 18, and 19) exhibited lower [O]/[C] ratios and moderate [H]/[C] ratios. This suggested that these samples had lower oxygen content and moderate hydrogen content, indicating their potential as efficient energy carriers. In combination with the pyrolysis conditions, higher pyrolysis temperatures (>600 °C) and cellulose percentages (>50 %) resulted in samples with lower [O]/[C] ratios and moderate [H]/[C] ratios, probably because higher pyrolysis temperatures promote the decomposition of cellulose and hemicellulose, releasing more gaseous and liquid products, which further increases the carbon content in the biochar while reducing its oxygen content. A higher cellulose content also contributes to the production of more carbonaceous products in the biochar, thereby increasing the [H]/[C] ratio and reducing the [O]/[C] ratio of the samples.

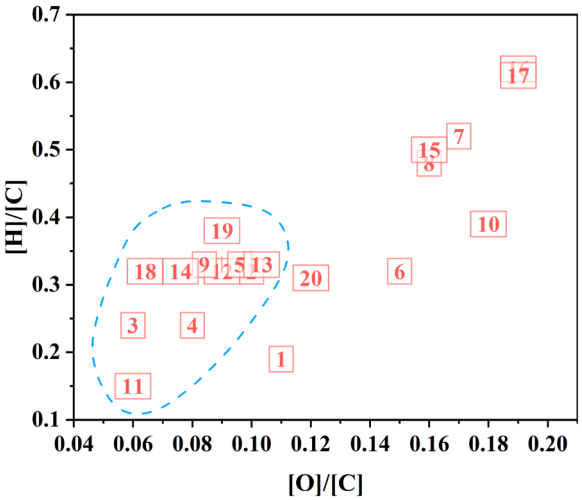

Fig. 4. Van-Krevelen diagram of biochar.

3.5. HHV analysis

The effect of co-pyrolysis interactions on HHV is shown in Fig. 5. Co-pyrolysis interactions led to an increase in HHV. The three conditions under which the interactions positively affected the carbon content can be summarized as follows: (1) at a fixed cellulose percentage of 50 %, temperatures ranging from 400.00 to 765.43 °C and times from 6.77 to 25.03 min (Fig. 5(a)); (2) at a fixed time of 17.5 min, temperatures ranging from 400.00 to 779.34 °C and cellulose percentages from 14.57 % to 98.05 % (Fig. 5(b)); (3) at a fixed pyrolysis temperature of 600 °C, a residence time from 7.71 to 24.33 min and a cellulose percentage from 17.76 % to 98.05 % (Fig. 5(c)). As displayed in Fig. 5(c), when the temperature was maintained at 600 °C, the SE value was the highest at 3.85 % at a time of 30.36 min and a cellulose percentage of 32.63 %. The co-pyrolysis interactions led to the highest HHV under these conditions because the interactions reduced the [O]/[C] ratio, which is a critical factor affecting the HHV of biochar. The [O]/[C] ratio and HHV are negatively correlated (Ahmad et al., 2012; Leng et al., 2021).

Eq. (9) is the model of biochar HHV. Increasing all three factors can contribute to a rise in HHV. The trends of the influence of the three factors on HHV were opposite to those for the [O]/[C] ratio, further illustrating the inverse relationship between HHV and the [O]/[C] ratio. This suggests that by fine-tuning the pyrolysis conditions such as temperature, residence time, and feedstock ratios, the [O]/[C] ratio of the biochar, which in turn directly affects its HHV, can be manipulated. This has notable implications for optimizing the energy characteristics of the biochar, making it more suitable for use as an efficient fuel or for other high-value applications.

$$HHV = +32.67 + 1.21A + 0.2444B + 0.6594C + 0.0491AB + 0.3781AC - 0.0982BC - 0.4571A^2 - 0.6728B^2 - 0.3528C^2 \quad (9)$$

3.6. Raman spectral analysis

In Raman spectroscopy analysis, the I_D/I_G ratio is an important indicator, where I_D and I_G represent the intensities of the defect peak (D peak) and the graphitic peak (G peak), respectively. The peak area ratio (I_D/I_G) is used to assess the graphitization degree of carbon materials, whereby a lower I_D/I_G ratio indicates a higher degree of graphitization. Co-pyrolysis interactions led to a reduction in the I_D/I_G values of the biochar. When the cellulose percentage was held constant while varying temperature and time, co-pyrolysis interactions had a dominant reducing effect on I_D/I_G. In contrast, when the time was constant and both cellulose percentage and temperature were varied, the effect of co-pyrolysis interaction on the reduction of I_D/I_G was secondary. As shown in Fig. 6(a), when the cellulose percentage was fixed at 50 %, the temperature was 541.94 °C, and the time was 22.74 min, the SE value was the lowest at 21.20 %. This indicated that the co-pyrolysis interactions under this set of conditions exhibited the strongest effect in lowering the I_D/I_G ratio while promoting the graphitization degree of the biochar to the greatest extent.

Eq. (10) is the model for the I_D/I_G ratio of biochar. An increase in

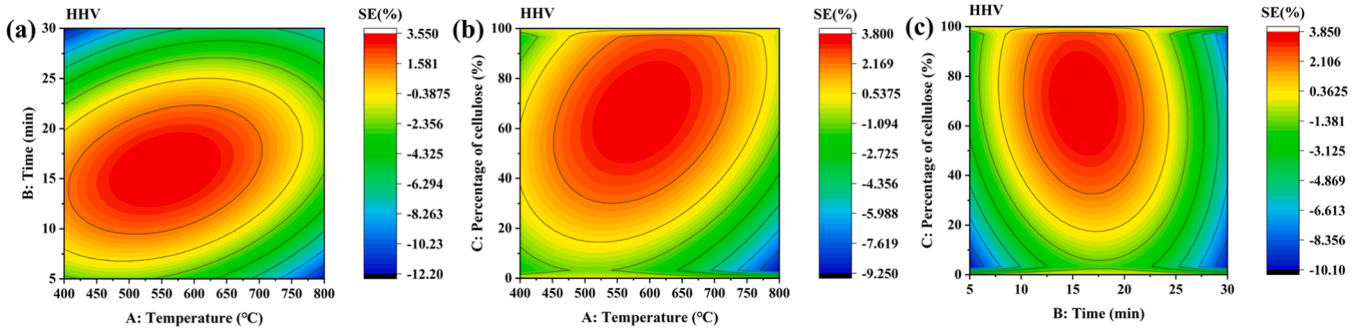

Fig. 5. The effect of co-pyrolysis interactions on HHV: (a) Temperature vs. time (cellulose percentage 50 %); (b) Temperature vs. cellulose percentage (17.5 min); (c) Time vs. cellulose percentage (600 °C).

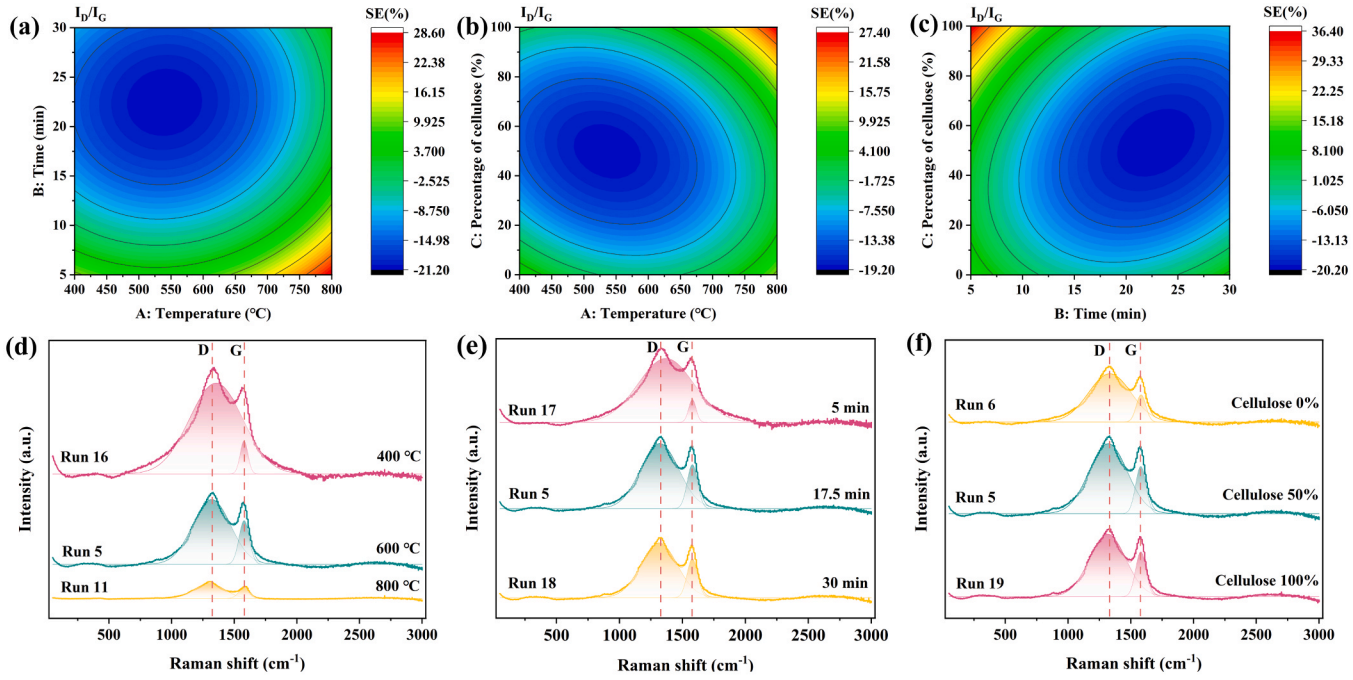

Fig. 6. Effect of co-pyrolysis interactions on I_D/I_G (a–c), and the Raman spectra of biochar (d–f): (a) temperature vs. time (cellulose percentage 50 %); (b) temperature vs. cellulose percentage (17.5 min); (c) time vs. cellulose percentage (600 °C); (d) pyrolysis temperature (17.5 min, cellulose percentage 50 %); (e) residence time (600 °C, cellulose percentage 50 %); (f) cellulose percentage (600 °C, 17.5 min).

temperature and time led to a reduction in the I_D/I_G values, while an increase in the cellulose percentage led to an increase in the I_D/I_G ratio. The rise in temperature and time causes hydrogen in the biochar to escape more readily as volatile compounds, while carbon tends to form stable backbone structures. This process contributes to the formation of more aromatic ring structures. As a possible reason for this trend, hemicellulose, which contains more complex and branched polysaccharides, tends to decompose into smaller molecules that can easily rearrange into aromatic structures during pyrolysis with the increase in temperature and time (Xu et al., 2020b). On the other hand, increasing the cellulose percentage reduces the biochar's aromaticity. In contrast, cellulose is a linear polymer primarily composed of glucose units and tends to form simpler, non-aromatic compounds during pyrolysis, leading to lower aromaticity in the resulting biochar compared to the biochar formed by hemicellulose (Gupta et al., 2016; Liao et al., 2022).

$$I_D/I_G = +7.91 - 5.27A - 2.14B + 1.47C + 0.4603AB - 0.4701AC - 0.3846BC + 1.19A^2 + 1.17B^2 + 0.1707C^2 \quad (10)$$

The Raman spectra of biochar are shown in Fig. 6(d)–(), which confirm the previous description. It can be concluded that raising the temperature and extending the time of pyrolysis decreases the I_D/I_G ratio of the biochar, while increasing the cellulose percentage increases the I_D/I_G ratio. Additionally, changes in pyrolysis temperature had a more significant effect on the I_D/I_G ratio than the variations in residence time and cellulose percentage. This indicates that pyrolysis temperature is the crucial factor for adjusting the aromaticity of biochar in practical applications (Zabaleta et al., 2024).

3.7. XPS analysis

3.7.1. C1s Peaks

The C 1 s XPS spectra of the biochar under different conditions, deconvoluted into three or four peaks, are shown in Fig. 7. The effect of co-pyrolysis interactions on C–C/C–H (C 1 s Peak I, located at 284.4 eV) is shown in Fig. 8(a)–(c) (Chen et al., 2022). The XPS C 1 s peaks results are shown in Table S4. In Fig. 8(a), at a cellulose percentage fixed at 50 %, lowering the temperature and prolonging the time led to higher SE values. This indicated that the co-pyrolysis interactions under these conditions strongly enhanced C 1 s Peak I. Fig. 8(b) shows that at a time of 17.5 min, raising the temperature and reducing the cellulose

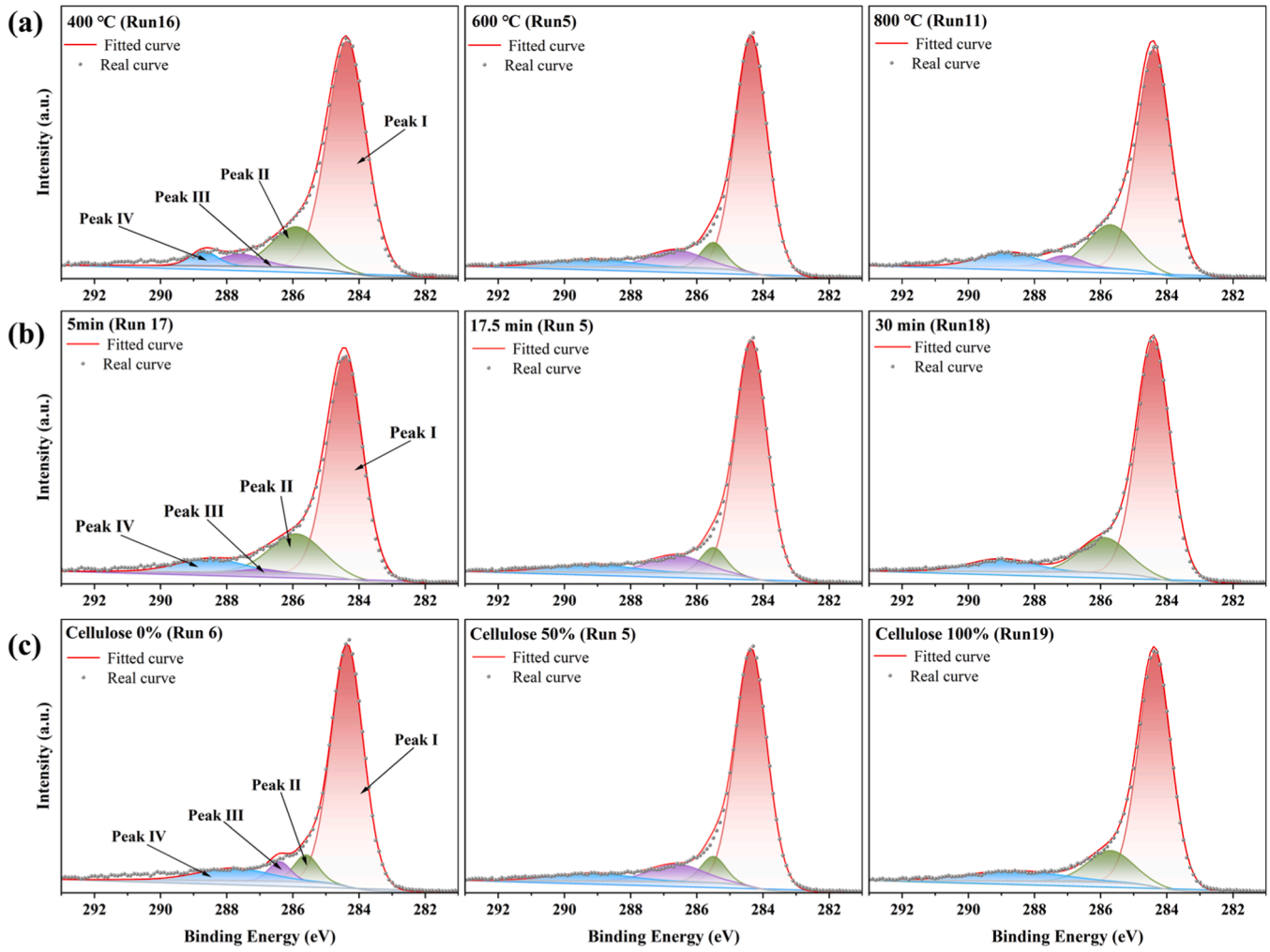

Fig. 7. C 1 s XPS peaks of biochar: (a) different pyrolysis temperatures (17.5 min, with 50 % cellulose percentage); (b) different residence times (600 °C, with 50 % cellulose percentage); (c) different cellulose percentage (600 °C, 17.5 min).

percentage resulted in higher SE values. In Fig. 8(c), when the temperature was set at 600 °C, extending the time and decreasing the cellulose percentage achieved higher SE values.

The effect of co-pyrolysis interactions on C–O/C–O–C (C 1 s Peak II), whose peak was located in the range of 285.9–286.2 eV, is shown in Fig. 8(d)–(f). Co-pyrolysis interactions led to an increase in the intensity of the C 1 s Peak II of biochar at a constant cellulose percentage. When the percentage of cellulose remained while time and temperature changed, the positive influence of co-pyrolysis interactions on the C 1 s Peak II was strong (Fig. 8(d)). At constant times and changing cellulose percentages and temperatures, the positive effect of co-pyrolysis interactions on the C 1 s Peak II was secondary (Fig. 8(e)). Under conditions of 50 % cellulose percentage, a pyrolysis temperature of 529.03 °C, and a residence time of 14.78 min, SE reached its highest value of 51.85 % (Fig. 8(d)). This indicated that under these conditions, the co-pyrolysis interactions demonstrated the strongest positive influence on C 1 s Peak II.

The effect of co-pyrolysis interactions on the C═O/COO– peak (C1s Peak III), located in the range of 285.9–286.2 eV, is illustrated in Fig. 8 (g)–(i). Co-pyrolysis interactions led to a reduction in the intensity of the C1s Peak III of the biochar. When the time was kept constant and temperature and cellulose percentage changed (Fig. 8(h)), the negative influence of the co-pyrolysis interactions on C 1 s Peak III was dominant but only secondary when varying cellulose percentage and time at a constant temperature (Fig. 8(i)). Among these conditions, i.e., a time of 17.5 min, a temperature of 438.71 °C, and a cellulose percentage of 50 % (Fig. 8(h)), the SE value was the lowest at 67.98 %, indicating that the co-pyrolysis interactions exhibited the strongest negative impact on C1s Peak III under these conditions.

The effect of co-pyrolysis interactions on the concentration of aromatic compounds (C 1 s Peak IV), whose peak was located between 288.8 eV and 289.5 eV, is shown in Fig. 8(j)–(l). It was observed that the co-pyrolysis interactions led to an increase in the intensity of the C 1 s Peak IV of the biochar. As depicted in Fig. 8(j), when the cellulose percentage was fixed at 50 %, lowering the temperature and shortening the time resulted in higher SE values, indicating that the co-pyrolysis interactions increased the intensity of C 1 s peak IV. In Fig. 8(k), lower temperatures combined with higher cellulose percentages led to increased SE values when the time was set at 17.5 min, suggesting a stronger enhancement of C 1 s Peak IV. Fig. 8(l) demonstrated that at a temperature of 600 °C, shorter times and higher cellulose percentages resulted in elevated SE values, indicating a more significant promotion of C 1 s Peak IV by the co-pyrolysis interactions.

The models for the four C 1 s XPS peaks of the biochar are represented by Eqs. (11), (12), (13), and (14). Increased pyrolysis temperature reduced the intensity of peaks I and IV but increased those of peaks II and III. Longer residence times enhanced the intensities of peaks I and III, while it reduced those of peaks II and IV. In contrast, an increase in cellulose percentage reduced the intensity of peaks I and III and increased the intensities of peaks II and IV.

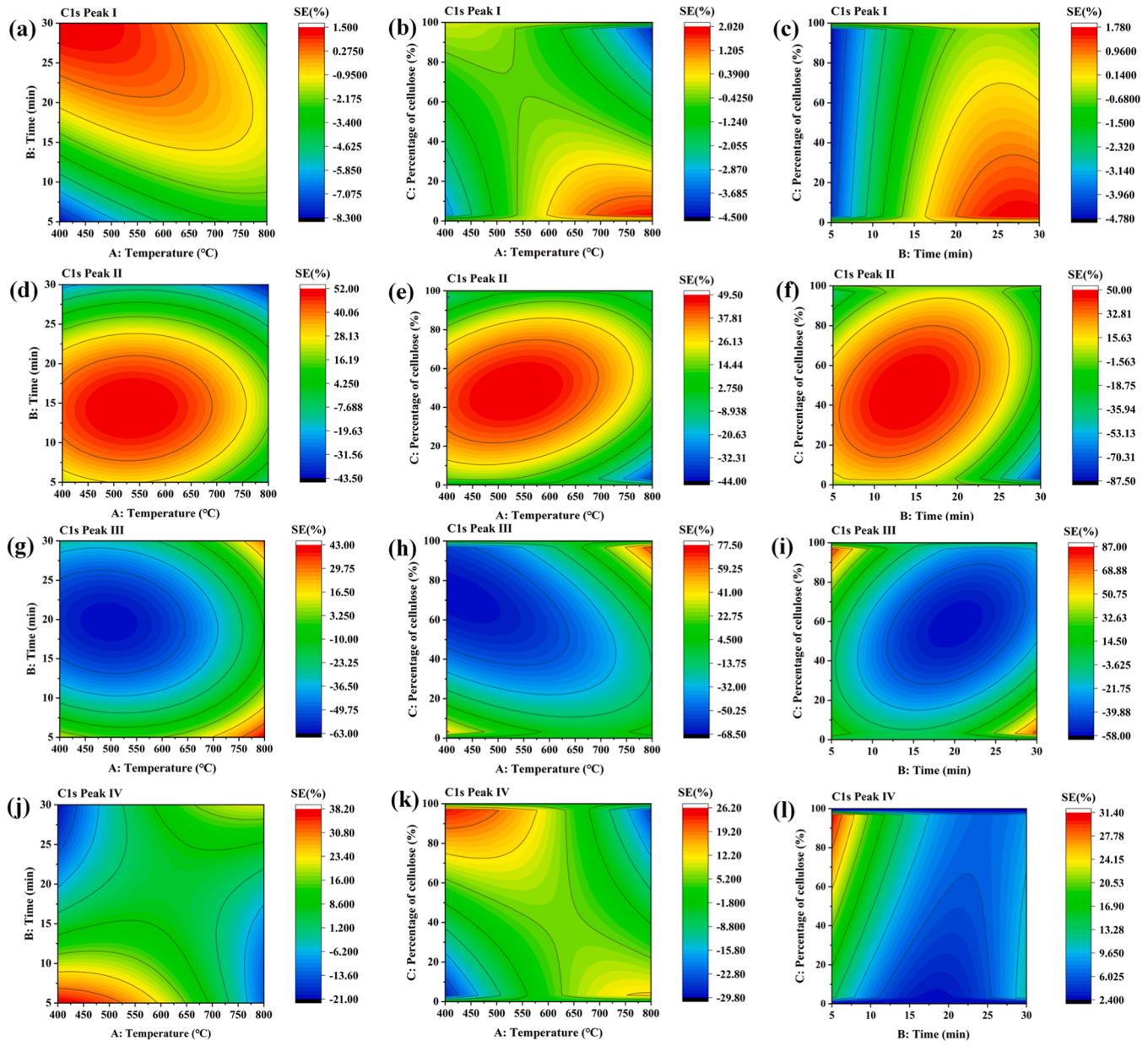

Fig. 8. Effect of co-pyrolysis interactions on (a)–(c) C–C/C–H (C 1 s Peak I), (d)–(f) C–O/C–O–C (C 1 s Peak II), (g)–(i) C═O/COO– (C 1 s Peak III) and (j)–(l) the concentration of aromatic compounds (C 1 s Peak IV) for (a), (d), (g), and (j) temperature vs. time (cellulose percentage 50 %), for (b), (e), (h), and (k) temperature vs. cellulose percentage (17.5 min), and for (c), (f), (i), and (l) time vs. cellulose percentage (600 °C).

$$\text{C1s Peak I} = +76.26 - 0.7289A + 1.27B - 1.40C + 1.31AB - 0.2652AC - 1.04BC - 0.9019A^2 - 0.7959B^2 + 0.7615C^2 \quad (11)$$

$$\text{C1s Peak II} = +15.82 + 0.0129A - 1.99B + 1.38C - 1.09AB - 0.6740AC + 0.9735BC + 0.3305A^2 + 0.4207B^2 - 2.15C^2 \quad (12)$$

$$\text{C1s Peak III} = +1.03 + 0.8795A + 0.7406B - 1.11C + 0.9354AB + 0.8814AC - 0.1228BC + 1.21A^2 - 0.0539B^2 + 0.5153C^2 \quad (13)$$

$$\text{C1s Peak IV} = +6.89 - 0.1645A - 0.0171B + 1.14C - 1.15AB + 0.0614AC + 0.1891BC - 0.6398A^2 + 0.4261B^2 + 0.8734C^2 \quad (14)$$

3.7.2. O1s Peaks

The O 1 s XPS spectra of biochar under different conditions, deconvoluted into three peaks, are shown in Fig. 9. The effect of co-pyrolysis interactions on the C═O peaks (O 1 s Peak I) located at 531.1 eV is illustrated in Fig. 10(a)–(c) (Li et al., 2024). The XPS O 1 s peaks results are shown in Table S4. The co-pyrolysis interactions exhibited varying effects on the intensity of O 1 s Peak I under the three test conditions. As shown in Fig. 10(a), when the cellulose percentage was fixed at 50 %, the SE value was the lowest at –61.64 % for a temperature of 800 °C and a time of 21.13 min, indicating that under these conditions, the co-pyrolysis interactions had the strongest inhibitory effect on the formation of C═O functional groups. As depicted in Fig. 10(c), at a constant temperature of 600 °C, a residence time of 5 min, and a cellulose percentage of 3.23 %, SE reached its maximum value of 27.38 %.

The effect of co-pyrolysis interactions on the OH peak (O 1 s Peak II) located at 532.6 eV is illustrated in Fig. 10(d)–(f). The conditions of the highest SE values indicated by the strongest effect on the OH peak intensity can be summarized as follows: (1) at a constant cellulose percentage of 50 %, a temperature of 554.84 °C, and a time of 17.90 min, the SE value was the highest at 20.19 % (Fig. 10(d)); (2) at a constant time of 17.5 min, a temperature of 567.74 °C, and a cellulose percentage of 45.16 %, SE reached its highest value of 20.31 % (Fig. 10(e)); (3)

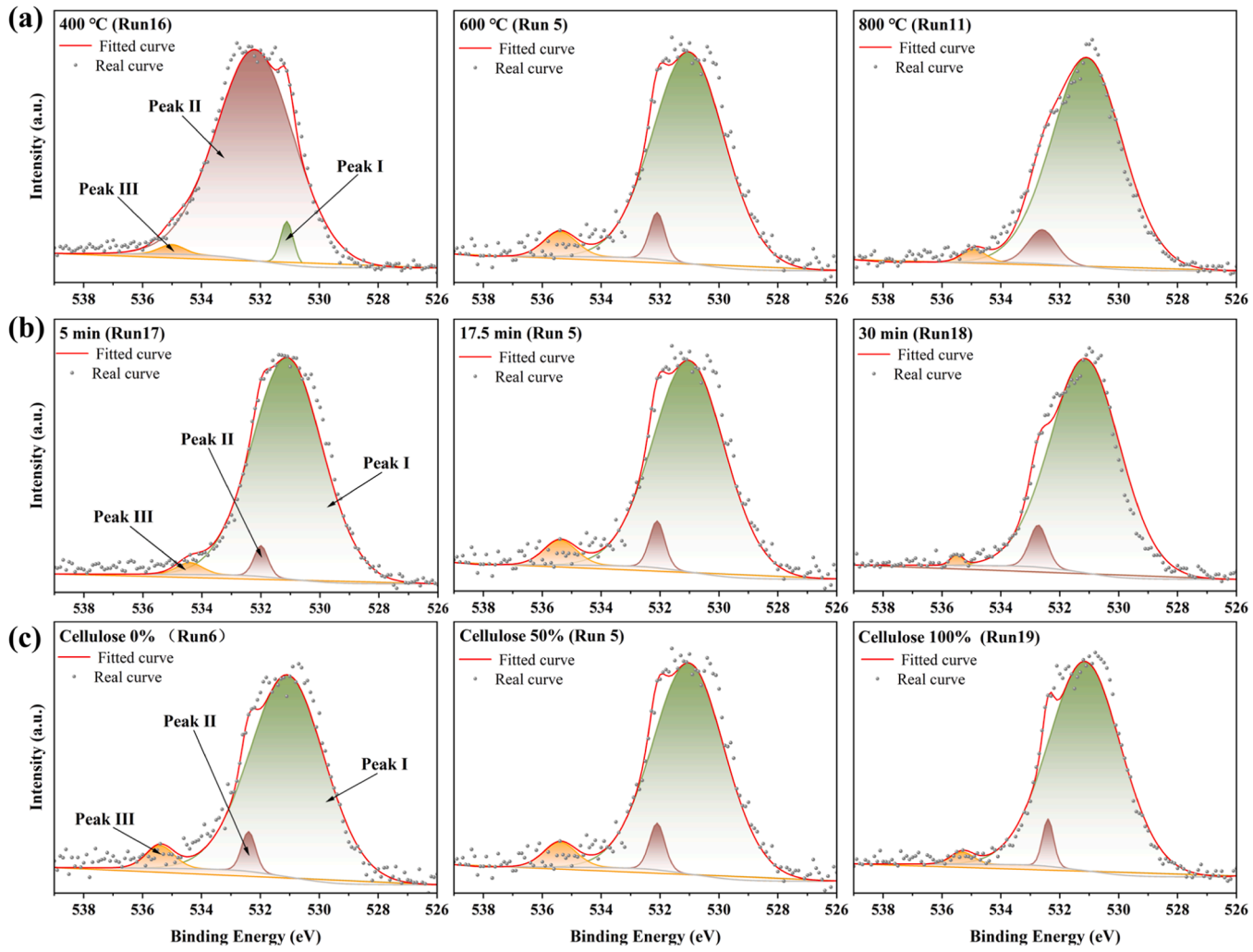

Fig. 9. Deconvoluted O 1 s XPS spectra of biochar: (a) different pyrolysis temperatures (17.5 min, with 50 % cellulose percentage); (b) different residence times (600 °C, with 50 % cellulose percentage); (c) different cellulose percentages (600 °C, 17.5 min).

when the temperature was fixed at 600 °C, SE reached its highest value of 19.89 % at a time of 16.92 min and a cellulose percentage of 38.71 % (Fig. 10(f)).

The effect of co-pyrolysis interactions on the COOH peak (O 1 s Peak III) located at 535.6 eV is illustrated in Fig. 10(g)–(i). The co-pyrolysis interactions had an inhibitory effect on COOH formation, leading to a decrease in peak intensity. When the cellulose percentage was held constant while varying temperature and time, the co-pyrolysis interactions had a strong reducing effect on the intensity of the O 1 s Peak III (Fig. 10(g)). In contrast, when the time was constant and both cellulose percentage and temperature were varied, the effect of co-pyrolysis interaction on the intensity reduction of the O 1 s Peak III was secondary (Fig. 10(h)). Among these conditions, when the cellulose percentage was 50 %, the SE value reached its lowest point at 72.79 % at a temperature of 464.52 °C and a time of 30 min (Fig. 10(g)), indicating that under these conditions, the co-pyrolysis interactions had the strongest inhibitory effect on the formation of COOH functional groups.

The models for the three O 1 s XPS peaks of biochar are represented by Eqs. (15), (16), and (17). An increase in pyrolysis temperature reduced the intensity of Peak II, while it enhanced the intensities of Peaks I and III. Extending the residence time decreased the intensity of Peaks I and III and enhanced that of Peak II. Raising the cellulose percentage reduced the intensity of Peaks II and III, while it increased that of Peak I.

$$\text{O1s Peak I} = +95.29 + 36.69A - 0.3075B + 0.5115C - 1.22AB + 0.2578AC + 0.7047BC - 22.51A^2 - 5.78B^2 - 6.20C^2 \quad (15)$$

$$\text{O1s Peak II} = +2.79 - 37.13A + 0.4362B - 0.2040C + 1.13AB - 0.2504AC - 0.7341BC + 22.79A^2 + 6.15B^2 - 6.04C^2 \quad (16)$$

$$\text{O1s Peak III} = +1.93 + 0.4421A - 0.1267B - 0.3070C + 0.0.872AB - 0.0061AC + 0.0331BC - 0.2802A^2 - 0.37566B^2 + 0.1582C^2 \quad (17)$$

3.8. Optimizing biochar as a potential energy vector

Biochar has a wide range of applications, especially as an energy vector. As indicated in previous sections, biochar produced by the co-pyrolysis of cellulose and hemicellulose exhibited a lower [O]/[C] ratio and a moderate [H]/[C] ratio. Furthermore, under the influence of the interaction between cellulose and hemicellulose during co-pyrolysis, the fixed carbon content, carbon content, and HHV of the biochar increased by 0.87 %, 3.60 %, and 3.85 %, respectively, suggesting that this interaction contributes to optimizing the properties of biochar as a potential energy vector.

4. Conclusion

The results obtained in this study indicated that the interactions of cellulose and hemicellulose during co-pyrolysis improved the yield and

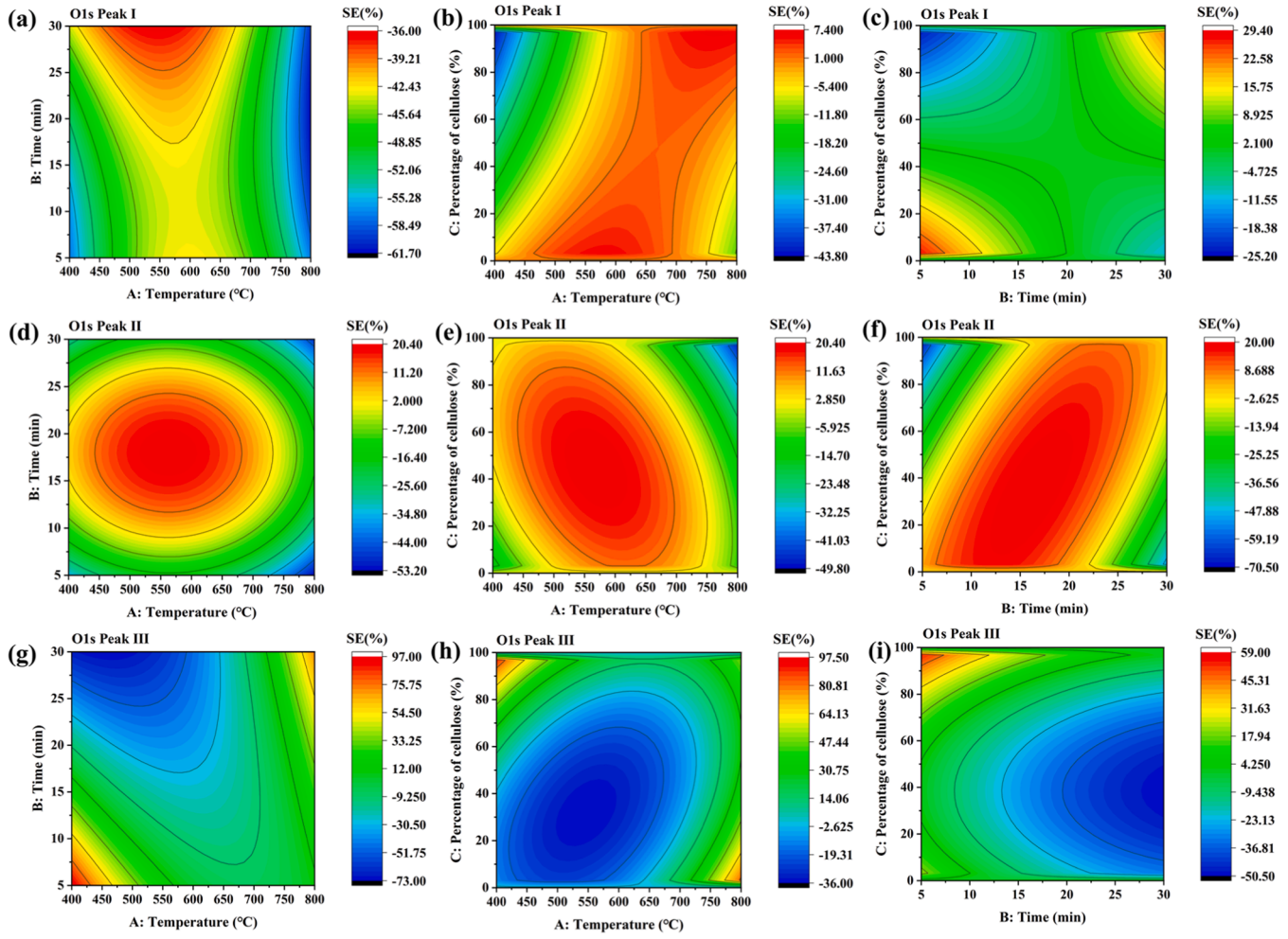

Fig. 10. Effect of co-pyrolysis interactions on (a)–(c) C═O (O 1 s Peak I), (d)–(f) OH (O 1 s Peak II), and (g)–(i) COOH (O 1 s Peak III) for (a), (d), and (g) temperature vs. time (cellulose percentage 50 %), for (b), (e), and (h) Temperature vs. cellulose percentage (17.5 min), and for (c), (f), and (i) time vs. cellulose percentage (600 °C).

performance of biochar. The co-pyrolysis interactions exhibited a positive impact on biochar yield, and the strongest positive influence reached 41.37 % SE (567.74 °C, 19.52 min, cellulose percentage of 50 wt%). Furthermore, the co-pyrolysis interactions were also beneficial for improving the fixed carbon content, carbon content, and HHV of the biochar, while reducing the volatile content, as well as [H]/[C] and [O]/[C] ratios. This was attributed to the melting of hemicellulose before cellulose during pyrolysis, generating a unique structure of cellulose covered by molten hemicellulose. This inhibited the production of cellulose volatiles, leading to an increase in solid residues. Additionally, Raman spectroscopy showed that the co-pyrolysis interactions negatively affected the peak area ratio I_D/I_G, indicating that the interaction enhanced the degree of graphitization of the biochar. XPS revealed that the co-pyrolysis interactions promoted the formation of C–C, C–O/C–O–C, aromatic rings, and OH functional groups while suppressing the formation of COO–, COOH, and C═O. These results indicated that the co-pyrolysis interaction between cellulose and hemicellulose contributed to optimizing the properties of biochar as a potential energy vector. This study provides a data foundation for applying biomass raw materials in the energy vector field.

CRediT authorship contribution statement

Dengyu Chen: Supervision, Funding acquisition. **Xiaoran Li:** Writing – original draft, Software. **Jinjin Li:** Data curation. **Kehui Cen:** Methodology. **Jiangyong Gao:** Visualization, Software. **Dongxia Jia:** Investigation. **Liqiang Zhang:** Writing – review & editing.

Declaration of Competing Interest

The authors declare that they have no known competing financial interests or personal relationships that could have appeared to influence the work reported in this paper.

Acknowledgements

This work was supported by National Key Research and Development Program of China (2023YFD2201602).

Appendix A. Supporting information

Supplementary data associated with this article can be found in the online version at doi:10.1016/j.indcrop.2024.120126.

Data availability

Data will be made available on request.

References

Ahmad, M., Lee, S.S., Dou, X., Mohan, D., Sung, J.-K., Yang, J.E., Ok, Y.S., 2012. Effects of pyrolysis temperature on soybean stover- and peanut shell-derived biochar properties and TCE adsorption in water. Bioresour. Technol. 118, 536–544. https://doi.org/10.1016/j.biortech.2012.05.042.

Amrullah, A., Farobie, O., Irawansyah, H., Lutfi, M., Haty, L.N., 2024. Synergistic enhancement of bio-oil production, quality, and optimization from co-pyrolysis purun tikus (Eleocharis dulcis) and plastic waste using response surface methodology. Process Saf. Environ. Prot. 187, 471–482. https://doi.org/10.1016/j.psep.2024.04.079.

Ba, Y., Cen, K., Wang, L., Jia, D., Kan, T., Chen, D., 2023. Study on synergistic effect of co-pyrolysis of wood chips and its gasification tar on the biochar and subsequent activated carbon upgrading using response surface method. Ind. Crops Prod. 205, 117558. https://doi.org/10.1016/j.indcrop.2023.117558.

Cai, B., Kang, R., Feng, J., Eberhardt, T.L., Ma, Z., Zhu, Q., Pan, H., 2024. Construction of Cu-Ru bimetallic catalyst for the selective catalytic transfer hydrogenation of carbonyl (C-O) in biomass-derived compounds. Renew. Energy 222, 119833. https://doi.org/10.1016/j.renene.2023.119833.

Cen, K., Chen, F., Chen, D., Gan, Z., Zhuang, X., Zhang, H., 2022. Life cycle assessment of torrefied cornstalk pellets combustion heating system. Fuel 320, 123968. https://doi.org/10.1016/j.fuel.2022.123968.

Chen, D.Y., Cen, K.H., Zhuang, X.Z., Gan, Z.Y., Zhou, J.B., Zhang, Y.M., Zhang, H., 2022. Insight into biomass pyrolysis mechanism based on cellulose, hemicellulose, and lignin: evolution of volatiles and kinetics, elucidation of reaction pathways, and characterization of gas, biochar and bio-oil. Combust. Flame 242, 112142. https://doi.org/10.1016/j.combustflame.2022.112142.

Chen, T., Li, L., Zhao, R., Wu, J., 2017. Pyrolysis kinetic analysis of the three pseudocomponents of biomass-cellulose, hemicellulose and lignin. J. Therm. Anal. Calorim. 128, 1825–1832. https://doi.org/10.1007/s10973-016-6040-3.

Couhert, C., Commandre, J.-M., Salvador, S., 2009. Failure of the component additivity rule to predict gas yields of biomass in flash pyrolysis at 950 °C. Biomass Bioenergy 33, 316–326. https://doi.org/10.1016/j.biombioe.2008.07.003.

Guo, Wj, Wang, Yr, Chen, W., Xu, Gx, Zhu, Gq, Xie, Gl, Xu, L., Fang, Z., Zhang, Q., Yang, H., 2024. Insight into the synergistic influence of nitrogen-doped biochar and NH_3 on selective production of 4-vinyl phenol from biomass catalytic pyrolysis by coupling catalyst in-situ regeneration. Ind. Crops Prod. 214, 118520. https://doi.org/10.1016/j.indcrop.2024.118520.

Gupta, N.K., Prakash, P., Kalaichelvi, P., Sheeba, K.N., 2016. The effect of temperature and hemicellulose-lignin, cellulose-lignin, and cellulose-hemicellulose on char yield from the slow pyrolysis of rice husk. Energy Sources Part A-Recovery Util. Environ. Eff. 38, 1428–1434. https://doi.org/10.1080/15567036.2014.941518.

He, D., Luo, Y., Zhu, B., 2024. Feedstock and pyrolysis temperature influence biochar properties and its interactions with soil substances: insights from a DFT calculation. Sci. Total Environ. 922, 171259. https://doi.org/10.1016/j.scitotenv.2024.171259.

Hosoya, T., Kawamoto, H., Saka, S., 2007. Cellulose-hemicellulose and cellulose-lignin interactions in wood pyrolysis at gasification temperature. J. Anal. Appl. Pyrolysis 80, 118–125. https://doi.org/10.1016/j.jaap.2007.01.006.

Hu, B., Zhang, W.M., Guo, X.-W., Liu, J., Yang, X., Lu, Q., 2024. Experimental and computational study on xylan pyrolysis: the pyrolysis mechanism of main branched monosaccharides. Fuel Process. Technol. 253, 107989. https://doi.org/10.1016/j.fuproc.2023.107989.

Kawamoto, H., 2015. Reactions and molecular mechanisms of cellulose pyrolysis. Mokuzai Gakkaishi 61, 1–24. https://doi.org/10.1016/j.fuproc.2023.107989.

Leng, E., He, B., Chen, J., Liao, G., Ma, Y., Zhang, F., Liu, S., Jiaqiang, E., 2021. Prediction of three-phase product distribution and bio-oil heating value of biomass fast pyrolysis based on machine learning. Energy 236, 125718. https://doi.org/10.1016/j.fuel.2022.125718.

Li, X., Cen, K., Wang, L., Jia, D., Zhu, X., Chen, D., 2024. Co-pyrolysis of cellulose and lignin: effects of pyrolysis temperature, residence time, and lignin percentage on the properties of biochar using response surface methodology. Ind. Crops Prod. 219, 119071. https://doi.org/10.1016/j.indcrop.2024.119071.

Liao, W., Zhang, X., Ke, S., Shao, J., Yang, H., Zhang, S., Chen, H., 2022. Effect of different biomass species and pyrolysis temperatures on heavy metal adsorption, stability and economy of biochar. Ind. Crops Prod. 186, 115238. https://doi.org/10.1016/j.indcrop.2022.115238.

Liu, J., Fu, H., Hu, B., Li, K., Zhao, L., Zhang, B., Lu, Q., Fu, Wy, 2023. Phosphorus-modified mesoporous niobium pentoxide catalyst for fast pyrolysis of cellulose to selective production of levoglucosenone. Ind. Crops Prod. 205, 117467. https://doi.org/10.1016/j.indcrop.2023.117467.

Ma, Y., Wang, C., Huang, Y., Zhu, X., 2024. Study on the effect of transition zone-condensation field for the evolution and selective condensation of biomass pyrolysis vapors. Fuel 368, 131614. https://doi.org/10.1016/j.fuel.2024.131614.

Mao, Y., Cai, B., Huang, M., Liu, X., Zhang, W., Ma, Z., 2023. A sustainable preparation strategy for the nitrogen-doped hierarchical biochar with high surface area for the enhanced removal of organic dye. Biochar 5, 1–20. https://doi.org/10.1007/s42773-023-00269-z.

Quan, C., Gao, N., Song, Q., 2016. Pyrolysis of biomass components in a TGA and a fixed-bed reactor: thermochemical behaviors, kinetics, and product characterization. J. Anal. Appl. Pyrolysis 121, 84–92. https://doi.org/10.1016/j.jaap.2016.07.005.

Singh, R.K., Shrivastava, D.K., Sarkar, A., Chakraborty, J.P., 2020. Co-pyrolysis of eucalyptus and sodium polyacrylate: optimization and synergistic effect. Fuel 277, 118115. https://doi.org/10.1016/j.fuel.2020.118115.

Torres-Sciancalepore, R., Nassini, D., Asensio, D., Bohe, A., Rodriguez, R., Fouga, G., Mazza, G., 2024. Synergistic effects of the mixing factor on the kinetics and products obtained by co-pyrolysis of Rosa rubiginosa rosehip seed and husk wastes. Energy Convers. Manag. 302, 118095. https://doi.org/10.1016/j.enconman.2024.118095.

Wang, C., Ma, Y., Zhu, X., 2023a. Effect of quantitative heat transfer performance on the separation and enrichment of bio-oil components during the selective condensation of biomass pyrolysis vapors. Fuel Process. Technol. 243, 118115. https://doi.org/10.1016/j.fuel.2020.118115.

Wang, J., Wei, M., He, J., Wang, Y., Ren, C., 2022. Optimization of repair process parameters for open-arc surfacing welding of grinding rolls based on the response surface method. Processes 10, 321. https://doi.org/10.3390/pr10020321.

Wang, S., Zhou, J., Zhang, Y., He, S., Esakkimuthu, S., Zhu, K., Kumar, S., Lv, G., Hu, X., 2023b. Biochar assisted cultivation of Chlorella protothecoides for adsorption of tetracycline and electrochemical study on self-cultured Chlorella protothecoides. Bioresour. Technol. 389, 129810. https://doi.org/10.1016/j.biortech.2023.129810.

Wang, Z., Xia, S., Wang, X., Fan, Y., Zhao, K., Wang, S., Zhao, Z., Zheng, A., 2024. Catalytic production of 5-hydroxymethylfurfural from lignocellulosic biomass: recent advances, challenges and opportunities. Renew. Sustain. Energy Rev. 196, 114332. https://doi.org/10.1016/j.rser.2024.114332.

Wu, Y., Deppermann, A., Havlik, P., Frank, S., Ren, M., Zhao, H., Ma, L., Fang, C., Chen, Q., Dai, H., 2023. Global land-use and sustainability implications of enhanced bioenergy import of China. Appl. Energy 336, 120769. https://doi.org/10.1016/j.apenergy.2023.120769.

Xing, B., Hu, Y., Xu, D., Li, B., Li, Y., Guan, W., Li, R., Wang, S., 2023. Recent advances and perspectives of copyrolysis of biomass and organic solid waste. Energy Fuels 37, 4769–4790. https://doi.org/10.1021/acs.energyfuels.2c03793.

Xu, Fx, Zhang, X., Zhang, F., Jiang, Lq, Zhao, Z.-l, Li, Hb, 2020a. TG-FTIR for kinetic evaluation and evolved gas analysis of cellulose with different structures. Fuel 268, 117365. https://doi.org/10.1016/j.fuel.2020.117365.

Xu, J., Liu, J., Ling, P., Zhang, X., Xu, K., He, L., Wang, Y., Su, S., Hu, S., Xiang, J., 2020b. Raman spectroscopy of biochar from the pyrolysis of three typical Chinese biomasses: a novel method for rapidly evaluating the biochar property. Energy 202, 117644. https://doi.org/10.1016/j.energy.2020.117644.

Yang, H., Yan, R., Chen, H., Lee, D.H., Zheng, C., 2007. Characteristics of hemicellulose, cellulose and lignin pyrolysis. Fuel 86, 1781–1788. https://doi.org/10.1016/j.fuel.2006.12.013.

Yang, X., Yuan, C., He, S., Jiang, D., Cao, B., Wang, S., 2023. Machine learning prediction of specific capacitance in biomass derived carbon materials: effects of activation and biochar characteristics. Fuel 331, 125718. https://doi.org/10.1016/j.fuel.2022.125718.

Zabaleta, R., Sanchez, E., Fabani, P., Mazza, G., Rodriguez, R., 2024. Almond shell biochar: characterization and application in soilless cultivation of Eruca sativa. Biomass Convers. Biorefinery 14, 17201–17218. https://doi.org/10.1007/s13399-023-04002-5.

Zalazar-Garcia, D., Celia Roman, M., Fernandez, A., Asensio, D., Zhang, X., Paula Fabani, M., Rodriguez, R., Mazza, G., 2022. Exergy, energy, and sustainability assessments applied to RSM optimization of integrated convective air-drying with pretreatments to improve the nutritional quality of pumpkin seeds. Sustain. Energy Technol. Assess. 49, 101763. https://doi.org/10.1016/j.seta.2021.101763.

Zalazar-Garcia, D., Fernandez, A., Cavaliere, L., Deng, Y., Soria, J., Rodriguez, R., Mazza, G., 2024. Slow pyrolysis of pistachio-waste pellets: combined phenomenological modeling with environmental, exergetic, and energetic analysis (3-E). Biomass Convers. Biorefinery 14, 9197–9215. https://doi.org/10.1007/s13399-022-03232-3.

Zhang, S., Mei, Y., Lin, G., 2024. Pyrolysis interaction of cellulose, hemicellulose and lignin studied by TG-DSC-MS. J. Energy Inst. 112, 101479. https://doi.org/10.1016/j.joei.2023.101479.

Zhao, B., O'Connor, D., Zhang, J., Peng, T., Shen, Z., Tsang, D.C.W., Hou, D., 2018. Effect of pyrolysis temperature, heating rate, and residence time on rapeseed stem derived biochar. J. Clean. Prod. 174, 977–987. https://doi.org/10.1016/j.jclepro.2017.11.013.

Zhao, L., Fu, H., Xia, Yg, Liu, J., Hu, B., Cheng, Zj, Luo, X., Yan, D., Li, Jh, Lu, Q., 2024. Coproduction of 1,4:3,6-dianhydro-α-d-glucopyranose, furfural, and formic acid through oxalic acid-assisted staged fast pyrolysis of cellulose. Energy Fuels 38, 4302–4311. https://doi.org/10.1021/acs.energyfuels.3c04958.

Zhou, X., Li, W., Mabon, R., Broadbelt, L.J., 2018. A mechanistic model of fast pyrolysis of hemicellulose. Energy Environ. Sci. 11, 1240–1260. https://doi.org/10.1039/c7ee03208k.

Zhu, L., Cai, W., Li, J., Chen, D., Ma, Z., 2024. Highly selective production of light aromatics from co-catalytic fast pyrolysis of pre-deoxygenated biomass and hydrogen-rich polyethylene using a dual-catalyst system. Energy 296, 121241. https://doi.org/10.1016/j.energy.2024.131241.